Effects of pore water-rock reaction on heat extraction from the karst geothermal reservoirs Based on the dual media model

Ji, Jiayan; Song, Xianzhi; Yi, Junlin; Song, Guofeng; Wang, Gaosheng

DOI
10.1016/j.energy.2024.130651

Publication date
2024

Document Version
Final published version

Published in
Energy

Energy 293 (2024) 130651

Contents lists available at ScienceDirect

Energy

journal homepage: www.elsevier.com/locate/energy

Effects of pore water-rock reaction on heat extraction from the karst geothermal reservoirs: Based on the dual media model

Jiayan Ji [a], Xianzhi Song [a,*], Junlin Yi [a], Guofeng Song [b], Gaosheng Wang [a]

[a] National Key Laboratory of Petroleum Resources and Prospecting, China University of Petroleum (Beijing), Beijing, 102249, China
[b] Department of Geoscience and Engineering, Delft University of Technology, Delft, 2628CN, the Netherlands

ARTICLE INFO

Handling editor: G Iglesias

Keywords:
Karst-based thermal reserve
Pore structure
Fracture aperture
Water-rock reaction
Thermal performance

ABSTRACT

Fractures and caves are the main flow and storage channels for the karst geothermal reservoirs, and the water-rock reaction within them significantly affects the thermal performance. Most previous studies concentrated on the fractures, disregarding the impact of the pore water-rock reaction. The objective of this study is to explore the importance of pore water-rock reactions and identify the influence of various parameters when considering pore and fracture water-rock reactions. A 3D thermal-hydraulic-chemical coupling model considering dual media of pores and fractures was developed. The importance of pore water-rock reactions is demonstrated, and quantitatively characterize the effect of injection temperature (T_{in}), injection rate (Q_{in}), injection concentration (c_{in}), and ratio of the reaction-specific surface area between pore and fracture (A_p/A_f) on the thermal performance. Results indicate that the pore water-rock reaction drastically affects the hydraulic conductivity and pressure difference, even leading to an opposite trend. The influence of water-rock reaction in pores on fracture deformation is regulated by A_p/A_f, which augments with A_p/A_f. The relative contribution of A_p/A_f to production temperature, net thermal power, pressure difference, and hydraulic conductivity are 12.8%, 4.1%, 6.8%, and 13.7%, respectively. This study provides a significant guide for accurate production prediction and exploitation of karst-based geothermal reservoirs.

1. Introduction

Geothermal energy is a renewable and clean energy source that has a significant impact on optimizing the energy structure, mitigating emissions, and promoting environmental sustainability [1]. There are abundant geothermal resources in China, of which high-temperature geothermal resources are mainly distributed in the Yunnan-Tibet geotropical region of southern Tibet, western Sichuan, and western Yunnan [2–5]. Low-temperature geothermal resources are widespread, and the North China Basin is particularly rich in medium-low-temperature geothermal resources [6]. There are abundant studies on geothermal resources in the Xiongan area during the next national 12th and 13th Five-Year Plan period, which have strongly supported the development and utilization of geothermal resources in the Xiongan area [7,8].

Geothermal reservoirs in the Xiongan area are mostly carbonate karst-type reservoirs, where large fractures and caverns are the main flow and storage channels of the reservoirs [7,8]. The production process is a complex thermal-hydraulic-mechanical-chemical multi--physical (THMC) field coupling process [9]. The working fluid is injected into the reservoir from the injection well, convective heat exchange with the reservoir, and then flows out from the production well. The stress, thermal, and chemical equilibrium of the reservoir are disrupted when the working fluid is injected into the reservoir, which induces stress variation and water-rock reactions, changing the morphology of pores and fractures and thus affecting the flow heat transfer processes inside the reservoir. Therefore, it is of great significance to investigate the effects of stress changes and water-rock reactions on the evolution of reservoir flow channels as well as thermal performance. Aiming at the influence of stress changes on the evolution of reservoir flow channels and thermal performance, abundant thermal-hydraulic-mechanical (THM) coupling models have been developed by previous studies [10,11]. The effects of poroelasticity [12], thermoelasticity [13], and thermal stress [11] on the evolution of reservoir flow channels and thermal performance have been studied. However, there are fewer studies on the effects of water-rock reactions on the evolution of reservoir flow channels and thermal performance.

Ontoy et al. [14] investigate the influence of injection parameters (injection temperature, silica concentration, pH, etc.) on amorphous

* Corresponding author.
E-mail address: songxz@cup.edu.cn (X. Song).

https://doi.org/10.1016/j.energy.2024.130651
Received 2 November 2023; Received in revised form 24 December 2023; Accepted 7 February 2024
Available online 8 February 2024

silica precipitation in the near-well region of the reservoir by THOUGHTREACT software. Xu et al. [15] explored mineral deposition in the area near the Nag-67 well in the Tiwi field, Philippines through the reaction transport model. The researcher found that amorphous silica precipitation occurred in a 10 m diameter area around the well, the porosity and permeability of the area were reduced and the pressure difference was increased. Rawal and Ghassemi et al. [16] proposed a THMC coupling model based on the finite element method (FEM) and boundary element method (BEM) to evaluate the effects of chemical reactions and stress on thermal performance. They found that the injection of low-temperature undersaturated water would induce the dissolution of silica in the reservoir, leading to an increase in fracture aperture. Laurent et al. [17] established a single-fracture model and a fracture-pore dual-medium model to investigate the effect of water-rock reaction on the permeability of the Soultz fracture. The findings indicate that the variation of pore permeability parameters is governed by the dissolution and precipitation of carbonates. The dissolution reaction occurred near the injection wells, leading to an increase in pore permeability parameters. The precipitation reaction occurred near the generation wells, causing a decrease in pore permeability parameters. The reactions in the pore have a significant influence on the general evolution of pore permeability parameters, indicating that the water-rock reaction in the pore cannot be neglected. Song and Pandey et al. [18–20] built a thermal-hydraulic-chemical (THC) coupling model to explore the evolution of fracture morphology under the water-rock reaction in the dry hot rock. It was found that fracture dissolution occurs with undersaturated injection, whereas fracture precipitation occurs with oversaturated injection. The injection rate has the most effect on thermal performance, while injection concentration significantly alters the fracture aperture. Chen et al. [21] constructed a THC coupling model considering multiple fractures embedded in the rock body based on the unified pipe network method. The influence of injection temperature, solution saturation, and pressure difference on the thermal performance of the system is investigated based on this model. The researcher discovered that the reaction rate accelerated with rising injection temperature. From previous studies, it can be seen that the water-rock reaction is known to affect the pore and fracture structure of the reservoir, which in turn affects the thermal performance of the system.

Especially, most previous studies have focused on dry-hot-rock, investigating the evolution of fracture morphology with the water-rock reactions, as well as the influence of the variation in fracture morphology on the thermal performance of the system. This is because fractures provide the most efficient access in most reservoirs. Whereas, there are abundant caves and fractures in the carbonate karst thermal reservoirs, which increase the reaction-specific surface area (The total area per unit mass of minerals involved in the reaction, which means the area of minerals contacted per unit volume of H2O under the background of this study.) and increase the reaction rate. Therefore, the water-rock reaction in the developmental caves of carbonate karst thermal reservoirs cannot be overlooked. Moreover, the influences of engineering and reservoir parameters on the thermal performance obtained from previous studies are distorted when considering the water-rock reactions in the dual medium of porous and fractured. Therefore, this paper establishes a thermal-hydraulic-chemical coupling model considering dual media of pores and fractures for the production process of karst-based geothermal reservoirs under water-rock action. The importance of water-rock reactions in the pore is demonstrated, and the effect of the ratio of the reaction-specific surface area between pore and fracture is investigated for the first time. Sensitivity evaluation is performed to quantitatively characterize the effect of each engineering and reservoir parameter on the heat extraction performance of the karst-based geothermal reservoirs. The key findings provide a significant guide for accurate production prediction and exploitation of karst-based geothermal reservoirs.

2. Model description

2.1. Model assumptions

This study aims to explore the importance of pore water-rock reactions and identify the influence of various parameters on thermal performance when considering the water-rock reaction in the pores and fracture. Reasonable assumptions are made: (1) Water is assumed to fill the reservoir as the working fluid. (2) This study only considers the water-rock reaction of carbonate rocks due to the target area being the Xiongan karst reservoir. (3) The variation of temperature caused by the reaction is ignored [22,23]. (4) The change of stress and the effect of stress on the porosity and fracture aperture are ignored in this study [24]. (5) The solutions in the reservoir are considered to be dilute solutions [25].

2.2. Governing equations

The thermodynamic and chemical balance inside the reservoir would be disturbed due to the injection of low-temperature fluid. That would lead to the water-rock reaction inside the reservoir, affecting the porosity and permeability of the reservoir, and thus affecting the thermal performance of the system. The fluid is injected into the reservoir from the injection well, extracting the heat from the reservoir, and flows out from the production well. Darcy's Law and heat transfer equations are adopted to describe the fluid flow and heat transfer process in reservoirs in this study. The temperature and concentration variation caused by the injection of low-temperature fluid disrupts the thermodynamic and chemical balance inside the reservoir, causing mineral dissolution and precipitation, which subsequently alters the pore and fracture structure in the reservoir. Transport equations and reaction kinetics equations were used to describe the mass transfer and reaction processes within the reservoir in this study. The control equations for the specific components are shown below:

Darcy's Law [26,27] is adopted to describe the fluid flow process within the reservoir, which is described by:

Porous rock matrix:

$$\frac{\partial(\varphi_p\rho_f)}{\partial t} - \nabla\cdot(\rho_f u) = -Q_f \tag{1}$$

$$u = -\frac{k_p}{\mu_f}(\nabla p + \rho_f g\nabla z) \tag{2}$$

Fracture:

$$d_f\frac{\partial(\varphi_f\rho_f)}{\partial t} - \nabla\cdot(d_f\rho_f u) = d_f Q_f \tag{3}$$

$$u = -\frac{k_f}{\mu_f}(\nabla p + \rho_f g\nabla z) \tag{4}$$

where φ_p and φ_f represent the reservoir matrix porosity and fracture porosity, respectively. ρ_f (kg/m^3) is the fluid density. k_p and k_f (m^2) are the pore permeability and the fracture permeability. p (Pa) represents the fluid pressure. μ_f (Pa·s) is the fluid dynamic viscosity. The item $\rho_f g\nabla z$ indicates the effect of gravity. d_f (m) denotes the fracture aperture. The parameter Q_f denotes the mass transfer between the rock matrix and fractures.

This study adopts the local thermal equilibrium model to control the heat transfer within the reservoir. The energy conservation equation is expressed as follows:

Porous rock matrix：

$$(\rho C_p)_{eff}\frac{\partial T}{\partial t} + \rho_f C_{p,f} u\cdot\nabla T - \nabla\cdot(\lambda_{eff}\nabla T) = -Q_{f,E} \tag{5}$$

Fracture：

$$d_f\left(\rho c_p\right)_{eff}\frac{\partial T}{\partial t}+d_f\rho_f c_{p,f}u\nabla(T)-\nabla\cdot\left(d_f\lambda_{eff}\nabla T\right)=d_f Q_{f,E} \tag{6}$$

where $(\rho c_p)_{\text{eff}}$ and λ_{eff} represent the effective volumetric capacity and the effective thermal conductivity, respectively. These are calculated by:

$$\left(\rho C_p\right)_{eff}=(1-\varphi)\rho_s C_{p,s}+\varphi\rho_f C_{p,f} \tag{7}$$

$$\lambda_{eff}=(1-\varphi)\lambda_s+\varphi\lambda_f \tag{8}$$

where ρ_s (kg/m3), $c_{p,s}$ (J/(kg·°C)), and λ_s (W/(m·°C)) indicate the density, heat capacity, and thermal conductivity of the reservoir solid component, respectively.

The solute transport process in the reservoir involves convection and diffusion, and the solute transport equation in the reservoir is presented below:

Porous rock matrix:

$$\frac{\partial\left(\varphi_p\rho_f c_{i,p}\right)}{\partial t}-D_i\nabla\left(\rho_f c_{i,p}\right)+u\cdot\nabla\left(\rho_f c_{i,p}\right)=\varphi_p R_i^{\,p} \tag{9}$$

Fracture:

$$d_f\left[\frac{\partial\left(\rho_f c_{i,f}\right)}{\partial t}-D_i\nabla\left(\rho_f c_{i,f}\right)+u\cdot\nabla\left(\rho_f c_{i,f}\right)\right]=d_f R_i^{\,f}+f_c \tag{10}$$

At interface:

$$\mathrm{f_C}=\left(\rho_{\mathrm{f}}c_{\mathrm{i,p}}-D_{\mathrm{i}}\frac{\partial\left(\rho_{\mathrm{f}}c_{\mathrm{i,p}}\right)}{\partial z}\right)_{z=-d_{\mathrm{f}}/2}-\left(\rho_{\mathrm{f}}c_{\mathrm{i,p}}-D_{\mathrm{i}}\frac{\partial\left(\rho_{\mathrm{f}}c_{\mathrm{i,p}}\right)}{\partial z}\right)_{z=d/2} \tag{11}$$

$$c_{i,p}\big|_{z=-d/2}=c_{i,p}\big|_{z=d/2}=c_{i,f} \tag{12}$$

where $c_{i,p}$ (mol/m^3) and $c_{i,f}$ (mol/m^3) are the concentration of substance "i" in the pore and fracture. D_i (m^2/s) represents the effective diffusion coefficient of substance "i" in the solution. $R_{i,p}$ and $R_{i,p}$ (mol/(m^3·s)) are the reaction rate in pore and fracture of substance "i", respectively. f_c represents the material transfer between matrix and fracture.

This paper mainly focuses on the water-rock reaction in the karst geothermal reservoir. Consequently, only the water-rock reaction process between carbonate rock and water is considered in this paper. Its chemical expression is displayed below:

$$H_2O_{(aq)}\Leftrightarrow H^+_{(aq)}+OH^-_{(aq)} \tag{13}$$

$$CaCO_{3(s)}+H^+_{(aq)}\Leftrightarrow HCO_3^-{}_{(aq)}+Ca^{2+}_{(aq)} \tag{14}$$

The chemical reaction is controlled by kinetics, and the reaction rate for the carbonate rock (R_{caco3}) is expressed as [17]:

$$R_{(CaCO_3)}{}^p=A_p k^+_{(CaCO_3)}\left(1-\frac{\mathrm{Q_{(CaCO_3)}}}{\mathrm{K_{eq(CaCO_3)}}}\right)\ \mathrm{R_{(CaCO_3)}{}^f}=A_f k^+_{(CaCO_3)}\left(1-\frac{Q_{(CaCO_3)}}{K_{eq\,(CaCO_3)}}\right) \tag{15}$$

$$k^+_{(CaCO_3)}=k^+_{(CaCO_3),25^\circ C}\times\exp\left[\frac{-E_a}{R}\cdot\left(\frac{1}{T}-\frac{1}{298.15}\right)\right] \tag{16}$$

$$Q_{(CaCO_3)}=\frac{\mathrm{a(Ca^{2+})}\times\mathrm{a(HCO_3^-)}}{\mathrm{a(H^+)}}\ SI=\frac{Q_{(CaCO_3)}}{K_{eq\,(CaCO_3)}} \tag{17}$$

$$\log\left(K_{eq(CaCO_3)}\right)=-850.098-0.1395T+\frac{46880.82}{T}+309.65\times\log(T)-\frac{2659139.928}{T^2} \tag{18}$$

where $k^+_{(CaCO3)}$ (mol/(m^2·s)) represents the reaction rate constants of carbonate. A_p (1/m) and A_f (1/m) are the specific surface areas of reservoir pores and fractures, respectively. It refers to the total area per unit mass of minerals involved in the reaction, which means the area of minerals contacted per unit volume of H_2O under the background of this study [28]. *Ea* (kJ/mol) and *R* (J/(mol·K)) are reaction activation energy and molar gas constant, respectively. $Q_{(CaCO3)}$ are ionic concentration product. *SI* represents the saturation index. $a(Ca^{2+})$ (mol/m^3), $a(HCO3^-)$ (mol/m^3), and $a(H^+)$ (mol/m^3) indicate the activity of calcium, bicarbonate and hydrogen ions, respectively. $K_{eq(CaCO3)}$ is the equilibrium constant of carbonate. Meanwhile, a positive reaction rate indicates dissolution reactions occur, and a negative reaction rate means precipitation reactions occur.

The pore and fracture structure of the reservoir deforms in response to the water-rock reaction, and the deformation relationship with the reaction rate is shown below [18]:

$$\frac{\partial\varphi_p}{\partial t}=\frac{R_{CaCO_3}{}^p M_{CaCO_3}}{\rho_{CaCO_3}}\ \frac{\partial d_f}{\partial t}=\frac{R_{CaCO_3}{}^f M_{CaCO_3}}{\rho_{CaCO_3}} \tag{19}$$

where M $_{\mathrm{CaCO3}}$ (kg/mol), and ρ_{CaCO3} (kg/m^3) represent molar masses and density of carbonate, respectively.

$$\mathrm{k_p}=\mathrm{k_0}\left(\frac{\varphi_{\mathrm{p}}}{\varphi_0}\right)^3\left(\frac{1-\varphi_0}{1-\varphi_{\mathrm{p}}}\right)^2\ \mathrm{k_f}=\frac{\mathrm{d_h}^2}{12} \tag{20}$$

$$d_h=d_{h0}+f_f\left(d_f-d_{f0}\right) \tag{21}$$

$$A_p=A_0\frac{\varphi_p}{\varphi_0}\frac{\log(\varphi_p)}{\log(\varphi_0)}\ A_f=\frac{1}{d_f} \tag{22}$$

where k_0 (m^2), φ_0, and A_0 (1/m) represent the initial permeability, initial porosity, and initial specific surface area of pores, respectively. d_h (mm) and d_{h0} (mm) are the hydraulic apertures and initial hydraulic apertures, respectively. d_f (mm) and d_{f0} (mm) indicate the fracture aperture and initial fracture aperture, respectively. f_f is the coefficient describing the transformation of two kinds of apertures. It refers to the irregularity of the fracture surface irregularity, with a typical range of 0.5–1 [29].

2.3. Geothermal productivity index

To reasonably characterize the thermal performance of the system, the production temperature T_{out} (°C), net thermal power *N* (MW), Injection-production pressure difference Δp (MPa), and hydraulic conductivity *K* (m/s) are proposed to indicate the thermal performance of the karst thermal reservoir. Net thermal power *N* (MW) is the difference between the output thermal power and the input thermal power, which is defined as:

$$N=\left(Q_{out}C_{p,f}{}^{out}\cdot T_{out}-Q_{in}C_{p,f}{}^{in}\cdot T_{in}\right)\times10^{-6} \tag{24}$$

where $C^{out}_{p,f}$ (J/(kg•K)) and $C^{in}_{p,f}$ (J/(kg•K)) are the specific heat capacity for the injection and production fluid, respectively. Q_{out} (kg/s) and Q_{in} (kg/s) are production rate and injection rate, respectively. The higher the *N*, the greater the thermal performance. The injection-production pressure difference Δp (MPa) represents the pressure required for a pump to maintain H_2O circulation, which is expressed by:

$$\Delta p=p_{in}-p_{out} \tag{23}$$

where p_{in} (MPa) and p_{out} (MPa) represent the injection and production pressure, respectively. The hydraulic conductivity *K* (m/s) indicates the impediments to the fluid flow in the reservoir, which is expressed by:

$$K=\frac{k\rho_f g}{\mu_f} \tag{25}$$

where *k* (m^2) indicates the reservoir permeability. *g* (m/s^2) is the gravitational acceleration.

3. Model solution

3.1. Computational model

In this study, the model is solved by COMSOL 6.0. Fig. 1 illustrates the computational model, which includes a 3D geothermal reservoir and fracture-cave developed reservoir (FCDR). The karst reservoir is mainly 2000 m underground. The karst reservoir is located 1000–2000 m underground. The geometric model is a 1000 m ×1000 m ×1000 m cube and the upper boundary is 1000 m far from the surface. The size of the reservoir is large enough to avoid boundary effects during production [30]. The FCDR is at the center of the karst reservoir and its dimensions are 500 m ×500 m ×500 m. The FCDR represents the highly permeable area (cave and fracture) within the reservoir and is the main spread range for heat extraction. Therefore, the cave and matrix in the FCDR are equated to a porous medium, and the connected fracture network in the FCDR is equated as one vertical and one horizontal fracture. The fracture length and height both are 500 m and the fracture is located at the center of the FCDR [31,32]. The initial fracture aperture is assumed as 1 mm. This is because the numerical simulation of the reservoir-scale triple--porosity model is still a challenging issue [33]. Meanwhile, the porosity and permeability in the FCDR are higher than that of the reservoir. More complex caves and fractures will be considered in the further study. An injection well and a production well are adopted in the FCDR. The diameter of the well is 0.1 m, the distance between the injection and production well is 400 m, and the length of the open hole is 500 m. Table 1 lists the parameters set in the reservoir, FCDR, fracture, and injection-production well.

3.2. Initial and boundary conditions

For the reservoir area, the initial temperature and pressure increase linearly from the top boundary to the bottom boundary. The temperature and pressure gradient are 0.012 °C/m and 0.01 MPa/m. The temperature and pressure at the top boundary are 60 °C and 14 MPa. The top, bottom, and side boundaries are considered to be the insulated and constant temperature conditions. The junction between the reservoir and the FCDR is set as the flux boundary. The fluid inside the reservoir and the FCDR tend to be in an equilibrium state and the solution is assumed to be neutral at the initial stage. The initial concentration of Ca^{2+} is 0.084 mol/m^3 (Equilibrium) and the initial pH value is 6.54. The injection concentration of Ca^{2+} is 0.01 mol/m^3 (Undersaturation) and the pH value is 7.52. For the FCDR area, the initial temperature and pressure setting are the same as for the reservoir. Chemical reactions and deformations occur mainly in this region. The injection well injection flow rate is 50 kg/s, and the production pressure is 20 Mpa. The simulation time is 30 years for this study. Table 2 lists the initial and boundary condition parameters for the base case.

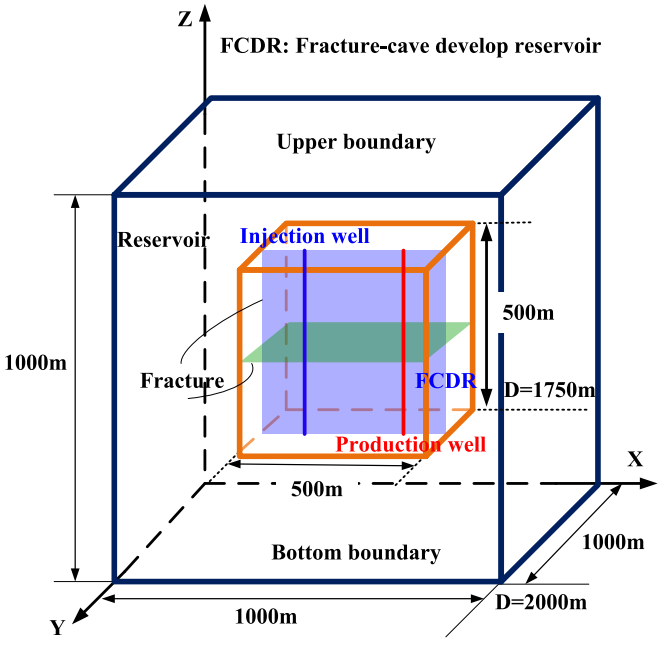

Fig. 1. Schematic representation of the computational model.

Table 1
The physical properties of fracture [34–36].

Items	Values
Density of the reservoir	2800 kg/m^3
Heat conductivity of the reservoir	3 W/(m·K)
Heat capacity of the reservoir	1000 J/(kg·K)
Porosity of the reservoir	0.01
Permeability of the reservoir	1×10^{-18} m^2
Density of the FCDR	2700 kg/m^3
Heat conductivity of the FCDR	2.8 W/(m·K)
Heat capacity of the FCDR	920 J/(kg·K)
Porosity of the FCDR	0.1
Permeability of the FCDR	30 mD
Density of the fracture	2000 kg/m^3
Heat conductivity of the fracture	2.8 W/(m·K)
Heat capacity of the fracture	850 J/(kg·K)
Porosity of the fracture	1
Initial fracture aperture	0.1 mm
Hydraulic aperture, d_{h0}	4×10^{-5} m
Coefficient of fracture irregularity, f_f	0.6
Initial specific surface area of pores, A_o	20000 1/m
Geothermal gradient	0.012 (K/m)
Wellbore diameter	0.1 m
Diffusion coefficient, D	1×10^{-9} m^2/s
Molar mass of carbonate	100 g/mol

3.3. Simulation mesh

Fig. 2 illustrates the meshing schemes. The FCDR is the main area where heat transfer and chemical reactions occur, the mesh in this region is intensive. The upper boundary of this region is divided into 28,976 sections by the free triangular mesh. Then this region is swept from top to bottom and divided into 289,760 sections. Finally, the free tetrahedral mesh method is adopted to divide the rest of the reservoir. Fig. 3 shows the variation of fracture aperture and porosity over 30 years of production under various finite mesh numbers. It can be seen that the fracture aperture and porosity almost stay constant when the mesh number exceeds 350,000. Therefore, the mesh number is conducted as 385,405 for the succeeding simulations.

3.4. Model validation

There is no experimental data or field data available for verification of the model. Therefore, an accurate analytic solution is a feasible and

Table 2
Initial and boundary conditions parameters for the base case [37,38].

Items	Values
Injection temperature	20 °C
Injection rate	50 kg/s
Production pressure	20 MPa
Temperature gradient	0.012 °C/m
Pressure gradient	10000 Pa/m
Temperature at the top of the boundary	60 °C
Pressure at the top of the boundary	14 MPa
Initial pH value	6.54
Injection solution pH value	7.52
Initial concentration of Ca^{2+}	0.084 mol/m^3
Injection concentration of Ca^{2+}	0.01 mol/m^3

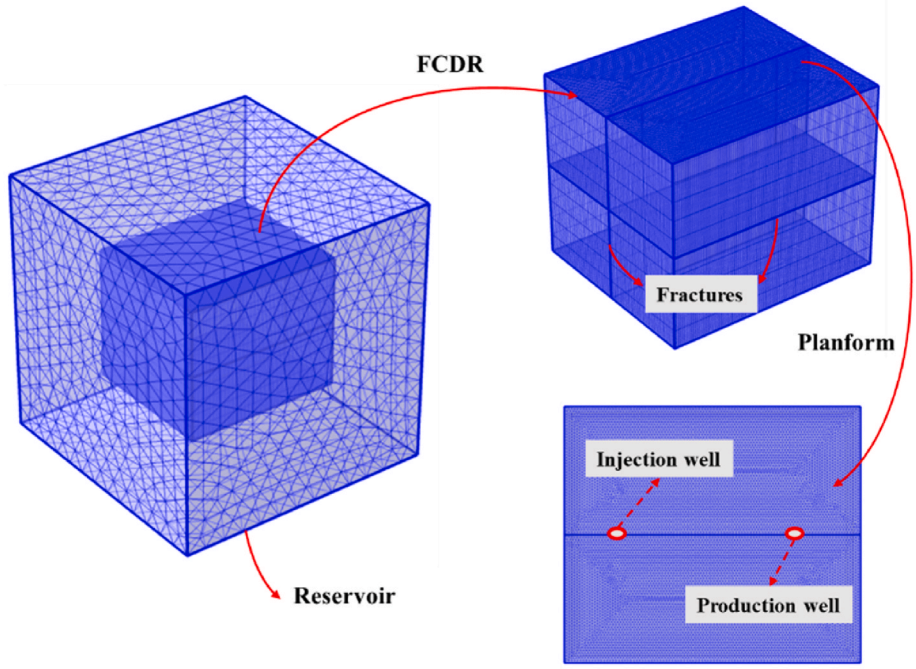

Fig. 2. Numerical meshing schemes.

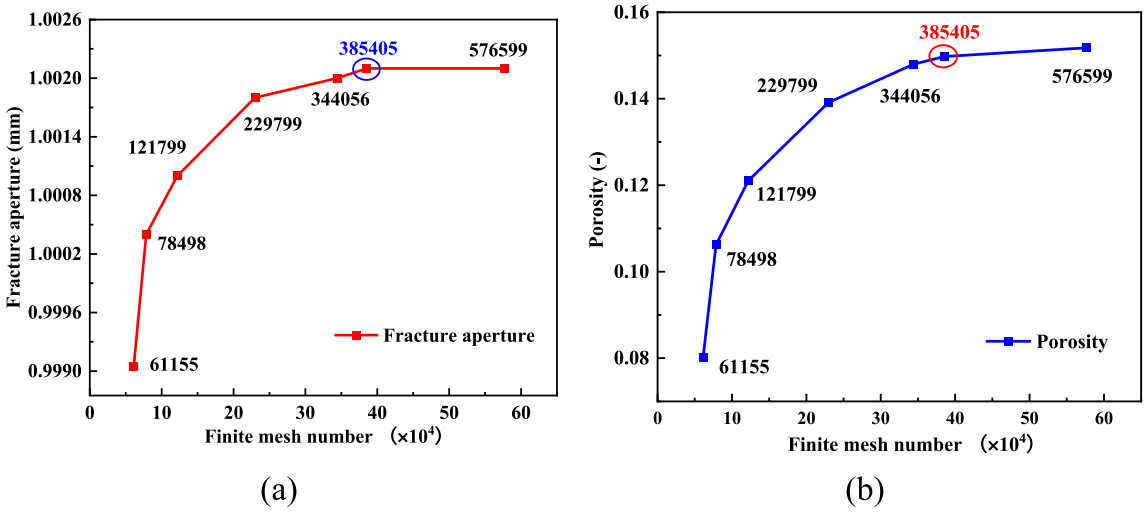

Fig. 3. Fracture aperture and porosity over 30 years of production under various finite mesh numbers.

reliable method to validate the THC coupling model. Due to the intricate THC coupling mechanism, the THC coupling model can be divided into TH, TC, and HC for separate validation. The TH coupling model is verified by the analytical solution for the fluid flow and heat transfer problems in a 2D infinite rock matrix with a single fracture [30,34]. TC coupling model is verified by the previous experiment and explores the influence of temperature on calcium carbonate reaction [39,40]. The HC coupling model is validated by the analytic model depicting solute tracks in the prescribed underground water flow field [41]. The analytical solution is represented by:

$$c_{\text{ana}} = \frac{M \times e^{\frac{\left\{-[(x-x_0)-ut]^2\times\left(2tD_{yy}+d^2\right)-[(y-y_0)-vt]^2\times\left(2tD_{xx}+d^2\right)+[(x-x_0)-ut]\times[(y-y_0)-vt]4tD_{xy}\right\}}{\left[8t^2\left(D_{xx}D_{yy}-D_{xy}{}^2\right)+2d^4+4d^2t\left(D_{xx}+D_{yy}\right)\right]}}}{2\pi ne\sqrt{4t^2\left(D_{xx}\times D_{yy}-D_{xy}{}^2\right)+d^4+2d^2t\left(D_{xx}+D_{yy}\right)}} \tag{26}$$

where M (mol/m^3) is the solute source. ne represents the effective porosity. x_0 and y_0 are the coordinates of the solute source, here x_0 equals −200 m and y_0 equals 200 m d (m) represents the width of the injection area. u (m/s) and v (m/s) indicate the horizontal and vertical velocity. D_{xx} (m^2/s), D_{yy} (m^2/s), and D_{xy} (m^2/s) are the dispersion tensor xx component, dispersion tensor yy component, and dispersion tensor xy component, respectively. The specific procedures for each model validation are described in the previous section [20,22]. Fig. 4 illustrates the comparison of results between numerical and analytical solutions of the HC coupled model and the maximum relative error is 6.6%. Therefore, the THC coupling model in this paper is vitrificated to be reliable due to the TH, TC, and HC coupling models have all verified their reliability. We have also compared our results with previous research cases in our previous study, which resulted in the same trend of variation [18,20,21]. The reliability of our model is further demonstrated.

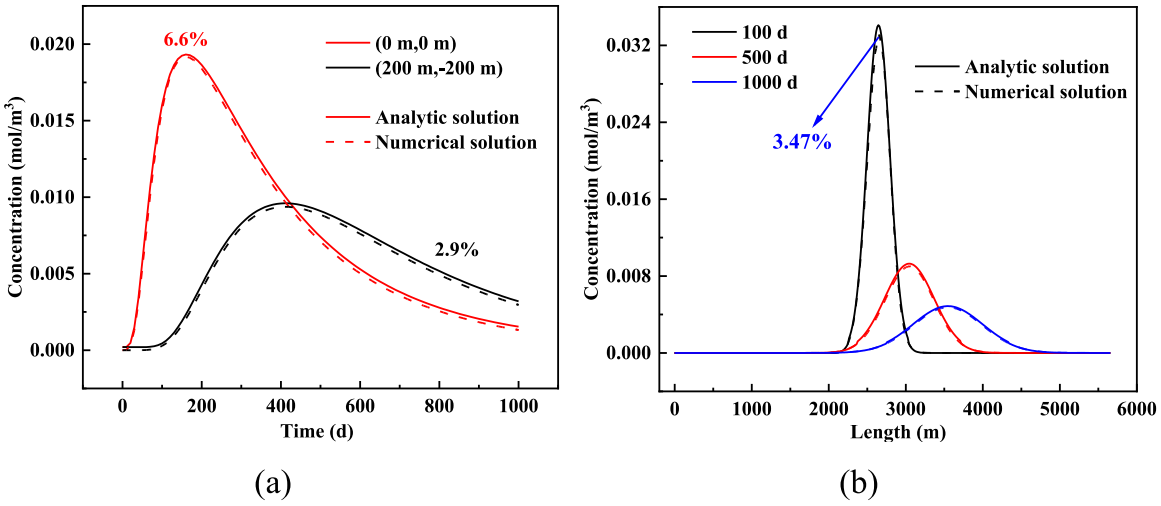

Fig. 4. The comparison of concentrations between analytical and numerical solutions results [41]: (a) at different positions, (b) along the diagonal line.

4. Results and discussions

4.1. The comparison with considering the water-rock reaction in pores and without

To explore the importance of the influence of water-rock reactions in pores on the pore and fracture deformation and thermal performance of the system. Fig. 5 illustrates the comparison of physical parameters between considering the water-rock reaction in pores and without after 15 years of production. Comparing the pressure distribution for the different cases, the pressure of the case without the water-rock reaction in pores is 25.3 MPa, which is less than that of the case considering the water-rock reaction in pores (30.7 MPa). The temperature distribution of the case considering the water-rock reaction in pores is similar to that of the case without considering the water-rock reaction in pores. However, the low-temperature swept area of the case considering the water-rock reaction in pores is greater than that of the without case. Comparing the concentration distribution for the different cases, there is a significant difference between the two cases. The calcium ion concentration near the injection well of the case considering the water-rock reaction in pores is 0.087 mol/m^3, which is much larger than the injection concentration. However, the calcium ion concentration near the injection well of the case without considering the water-rock reaction in the pore is 0.01 mol/m^3, which is equal to the injection concentration. This means that water-rock reactions in the pores near the injection well would cause the reservoir concentration to rapidly converge to the equilibrium concentration and at a faster reaction rate than water-rock reactions within the fracture. There is a significant difference in the distribution characteristics of fracture apertures when considering the water-rock reaction in the pore compared to not considering that. The fracture aperture at the injection well for the case of considering the water-rock reaction in the pore increased by 0.15% at year 15, while the fracture aperture at the injection well for the case of without considering the water-rock reaction in the pore increased by 71.48%. Further comparing the concentration distribution, it can be concluded that the water-rock reaction in the pore not only affects the variation of pore structure but also affects the concentration distribution in the reservoir (so that the concentration in the near-well region changes from the injected concentration to the equilibrium concentration). The variation of concentration would change the reaction mechanism at the fracture

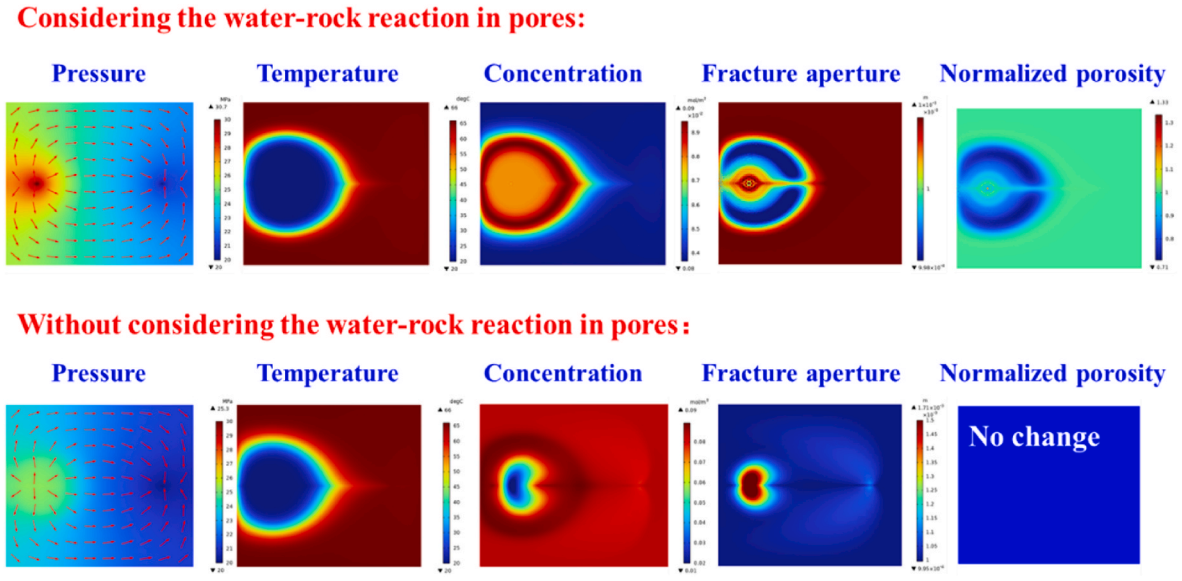

Fig. 5. The comparison of physical parameters between considering the water-rock reaction in pores and without after 15 years of production (a) pressure, (b) temperature, (c) concentration, (d) fracture aperture, (e) normalized porosity.

(Concentration difference, temperature difference double drive to temperature difference drive [22]), affecting the water-rock reaction on the fracture and fracture deformation. The distribution of normalized porosity is similar to the fracture aperture distribution. The normalized porosity at the injection well for the case of considering the water-rock reaction in the pore increased by 13.35% at year 15. The normalized porosity for the case without considering the water-rock reaction in the pore is not changed.

Further exploring the effect of water-rock reactions in the pore on the thermal performance of the system. Fig. 6 shows the comparison of thermal performance between considering the water-rock reaction in pores and without. Comparing these thermal performance indexes, we can see whether or not considering the water-rock reaction in the pores has little effect on the production temperature and net thermal power. After 30 years of production, the production temperature and net thermal power were reduced by 4.9% and 6.01% for the case considering the water-rock reaction in the pores, and the production temperature and net thermal power were reduced by 5.4% and 8.06% for the case without. This is due to the abundance of pore-fractures in karst reservoirs and the extensive thermal ripple area of the system, which has stable and efficient heat transfer properties. This conclusion is also consistent with the field results of the Soultz geothermal field [17,35].

On the contrary, there is a greater influence of the water-rock reaction in the pore on the injection-production pressure difference and hydraulic conductivity. The Δp increased by 66.62% for the case considering the water-rock reaction in the pores. whereas, the Δp decreased by 35.16% for the case without. The reservoir hydraulic conductivity decreased by 31.03% for the case considering the water-rock reaction in the pores and increased by 16.14 times for the case without. From the above analysis, it can be seen that the water-rock reaction in the pore has a drastic effect on the reservoir hydraulic conductivity and the system injection-production pressure difference, even leading to an opposite trend. This is because the water-rock reaction in pores near the injection well rapidly changes the solution concentration from the injected concentration to the equilibrium concentration, thus changing the reaction mechanism at the fracture surface and affecting the reaction and deformation of the fracture. In summary, the water-rock reaction in the pores of the karst thermal reservoir should not be neglected, and it has a significant impact on the reservoir pore and fracture deformation and heat extraction performance.

4.2. Effect of key factors

From the above analysis, it is clear that the water-rock reaction in the

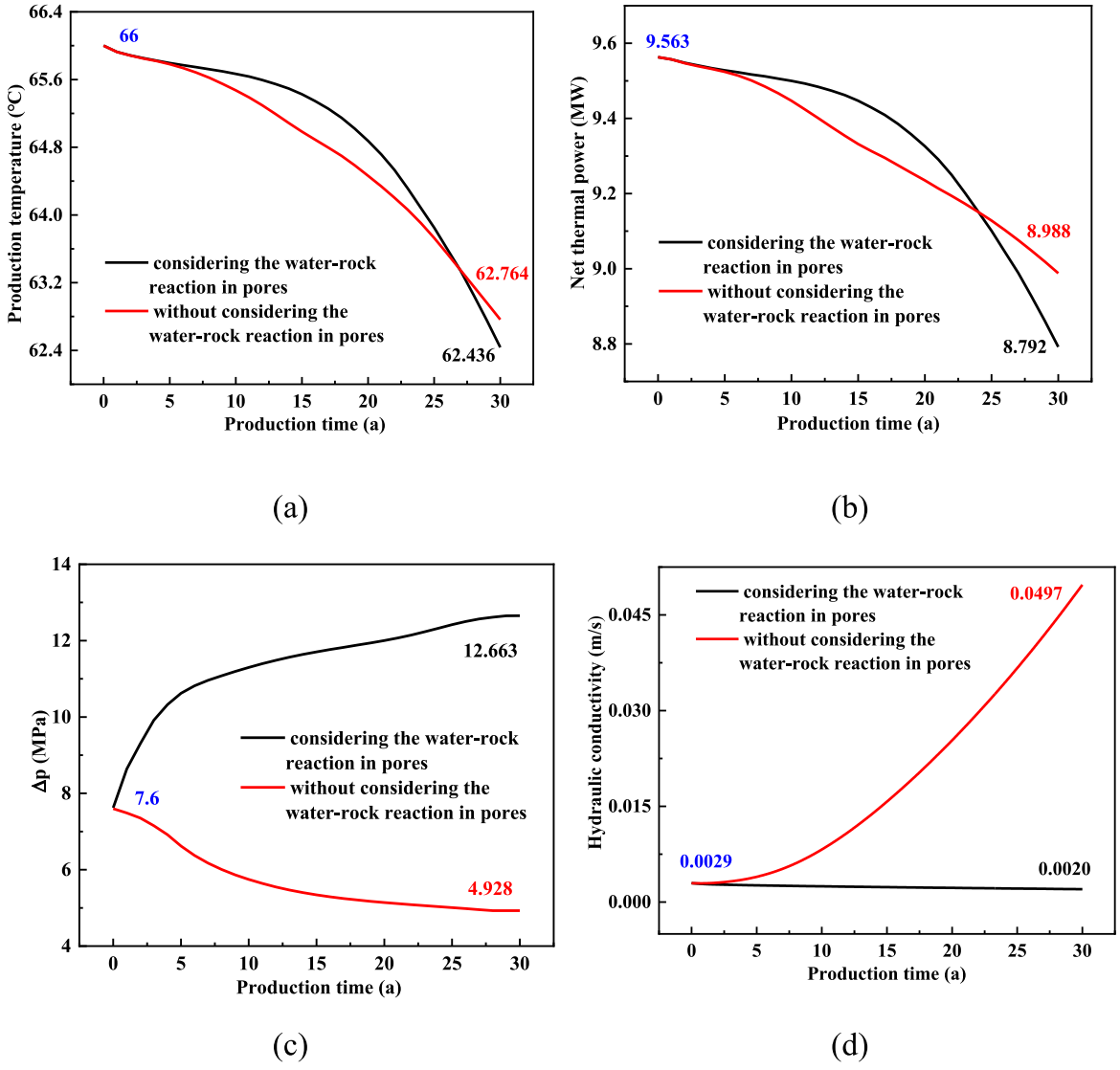

Fig. 6. The comparison of thermal performance between considering the water-rock reaction in pores and without, (a) production temperature, (b) net thermal power, (c) Injection-production pressure difference, and (d) Hydraulic conductivity.

pores of the karst thermal reservoir has a significant impact on thermal performance. According to Eqs. (9)–(19), the influencing factor that leads to the different chemical reactions within the pores and fractures is the reaction-specific surface area. Therefore, it is necessary to investigate the effects of the ratio of the reaction-specific surface area between pore and fracture (A_p/A_f) and injection parameters (injection temperature, rate, and concentration) on the thermal performance of the system. This would be a significant guide for the production of the karst thermal reservoir. Table 3 lists the paraments settings for the 20 cases where the bold paraments indicate the base case. Separate qualitative and quantitative analyses will be performed to investigate the effect of each parameter on thermal performance. Thermal performance evaluation indexes follow section 2.3.

4.2.1. The effect of injection temperature

The saturation index and fluid thermophysical properties are sensitive to the temperature. Here, the effect of injection temperature on the thermal performance is explored. The change in thermal performance index over time at different T_{in} is shown in Fig. 7. The production temperature decreases with time and the lowest production temperature is achieved when the injection temperature is 30 °C. However, the values of the production temperature are similar for different injection temperatures. The pressure difference rises with time and decreases with the injection temperature. This is because the fluid kinetic viscosity decreases with the injection temperature, thus reducing the resistance to flow. The net thermal power decreases with time and rapidly decreases with injection temperature. This will be explained in more detail below. The hydraulic conductivity reduces with time, which means the precipitation reactions occur in the reservoir as production proceeds, resulting in a decrease in reservoir permeability. The hydraulic conductivity increases with the injection temperature, which suggests that higher injection temperatures weaken the precipitation reactions in the reservoir.

Further quantitative investigation of the effect of injection temperature on the thermal performance, Fig. 8 shows the variation of (a) production temperature and pressure difference, and (b) net thermal power and Hydraulic conductivity with different T_{in} after 30 years. The injection temperature has a small effect on the production temperature. The production temperature is reduced by 0.43% when the injection temperature increases from 10 °C to 30 °C, and the production temperature is raised by 2.29% when the injection temperature increases from 30 °C to 50 °C. It can be seen that the effect of injection temperature on production temperature is complex, but the effect is little and largely negligible. The pressure difference is decreased by 40.57% and the hydraulic conductivity is raised by 40.18% when the injection temperature increases from 10 °C to 50 °C. This means that higher injection temperatures weaken the precipitation reactions, reducing the resistance to fluid flow in the reservoir. This is caused by the fluid dynamic viscosity decreasing with temperature. Meanwhile, the temperature difference between the fluid and reservoir reduces with injection temperature, weakening the water-rock reactions in the reservoir [22]. The net thermal power is decreased by 72.77% when the injection temperature increases from 10 °C to 50 °C. This is because the production temperature is similar for different injection temperatures, but the specific heat capacity for the injection solution increases with the injection temperature. According to Eq. (24), the net thermal power decreases with the injection temperature. From the above analysis, it can be seen that the injection temperature has a greater impact on the pressure difference, net thermal power, and hydraulic conductivity, and a little impact on the production temperature.

Table 3
The settings of case paraments.

Parameters	Values
T_{in} (Injection temperature (°C))	10, **20**, 30, 40, 50
Q_{in} (Injection rate (kg/s))	30, 40, **50**, 60, 70
c_{in} (Injection concentration (mol/L))	0, **0.01**, 0.084, 0.1, 0.2
A_p/A_f (Ratio of A_p and A_f (−))	0.05, 0.5, 1, 2, **20**

4.2.2. The effect of injection rate

The injection rate affects the flow velocity in the reservoir and affects the thermal performance of the system. The variation of the thermal performance index over time at different Q_{in} is shown in Fig. 9. The production temperature decreases with time and decreases with the injection rates. This is because high injection rates accelerate the spread of the low-temperature region. The pressure difference rises with time and increases with the injection rate. This is due to the need to increase the circulating pressure with the injection rate to ensure stable production. The net thermal power decreases with time and increases with the injection rate. It is the opposite of the variation of temperature with injected rates. The higher injection rates result in lower production temperatures but obtain higher net thermal power. This is due to the net thermal power is proportional to the injection rate. However, the degree of decrease in net thermal power with time increases with the injected rate. This means that we have to reasonably optimize the injection rate, not more is better. The hydraulic conductivity reduces with time and decreases with the injection rate. This means that the higher injection rates enhance the precipitation reactions and increase the resistance to flow in the reservoir.

Fig. 10 quantitatively illustrates the variation of thermal performance with different injection rates after 30 years. The production temperature is reduced by 10.90% when the injection rate increases from 30 kg/s to 70 kg/s. This means that higher injection rates accelerate the spread of low-temperature fluid regions thus accelerating the occurrence of thermal breakthrough. The pressure difference is increased by 154.98% whereas the hydraulic conductivity is reduced by 20.15% when the injection temperature increases from 30 kg/s to 70 kg/s. This means that more pressure is needed with the increase of injection rates to ensure a stable flow. Meanwhile, the higher injection rates increase the low-temperature spread area and enhance the precipitation reactions in the reservoir [22]. The net thermal power is increased by 94.81% when the injection temperature increases from 30 kg/s to 70 kg/s. This is due to the positive correlation between net thermal power and injected rate, as shown in Eq. (24). From the above analysis, it can be seen that the injection rate has a greater impact on each parameter (production temperature, pressure difference, net thermal power, and hydraulic conductivity). Therefore, it is recommended to rationally optimize the injection rate during the production process.

4.2.3. The effect of injection concentration

The injection concentration affects the saturation state of the solution in the reservoir and thus determines the direction in which the reaction occurs. The variation of the thermal performance index over time at different c_{in} is shown in Fig. 11. The production temperature decreases with time and increases with the injection concentration. However, the injection concentration has little effect on the production temperature, the production temperature is just increased by 0.66% when the injection concentration increases from 0 mol/L to 0.2 mol/L. This is because the water-rock reaction in the pore rapidly changes the solution concentration from the injected concentration to the equilibrium concentration, resulting in both undersaturated and oversaturated injections only affecting the area near the injection well. Therefore, the injection concentration has little effect on the production temperature in the case of this study. The pressure difference rises with time and increases with the injection concentration. This is due to the conversion from undersaturated to supersaturated injection near the injection well with the injection concentration increases, which induces a change from a dissolution reaction to a precipitation reaction near the injection well thus leading to an increase in the pressure difference. The net thermal power decreases with time and increases with the injection concentration. However, the injection concentration has little effect on the net

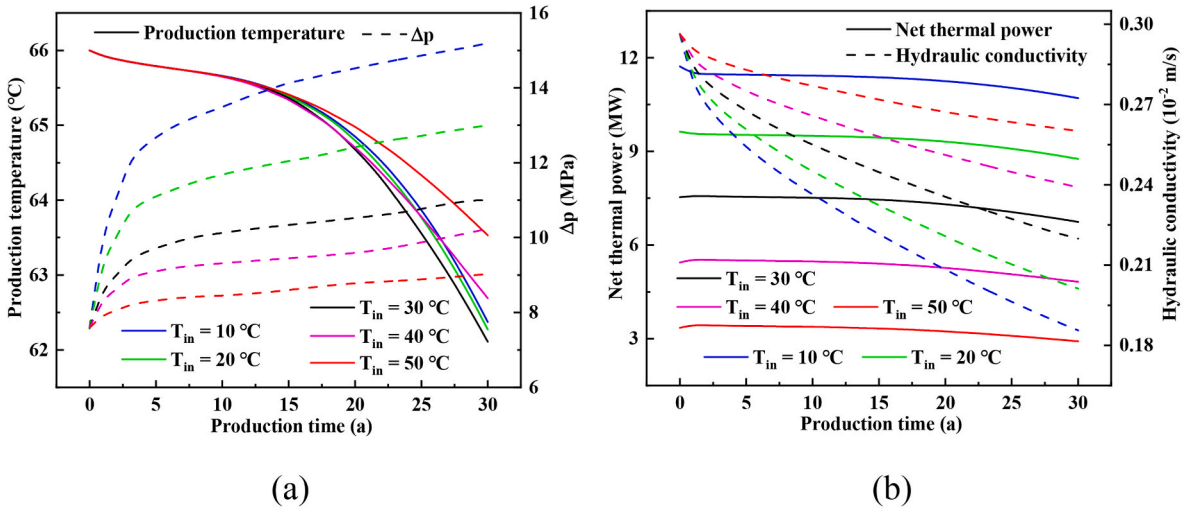

Fig. 7. The variation of (a) production temperature and pressure difference, and (b) net thermal power and Hydraulic conductivity with time at different T_{in}.

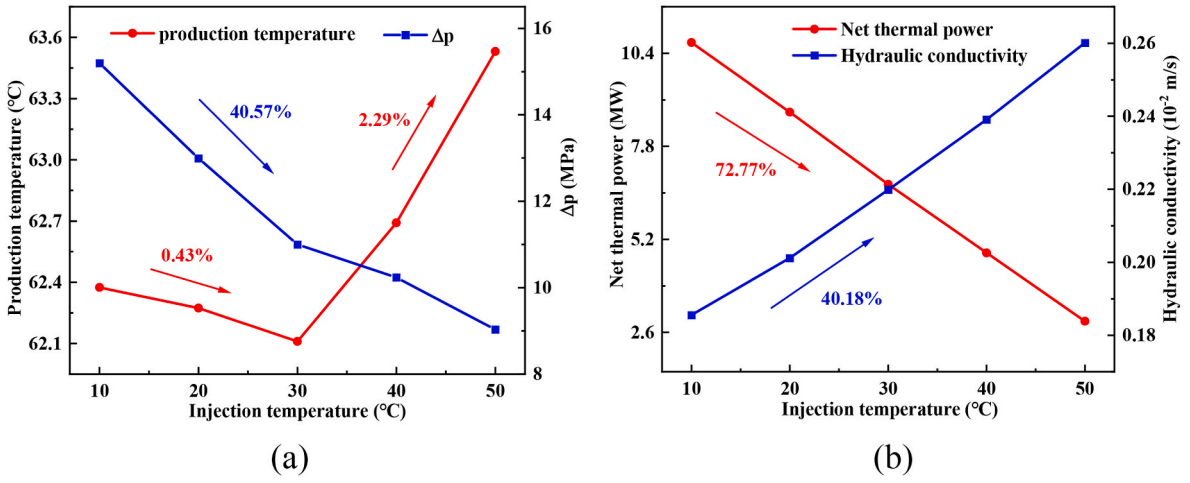

Fig. 8. The variation of (a) production temperature and pressure difference, and (b) net thermal power and Hydraulic conductivity with different T_{in} after 30 years.

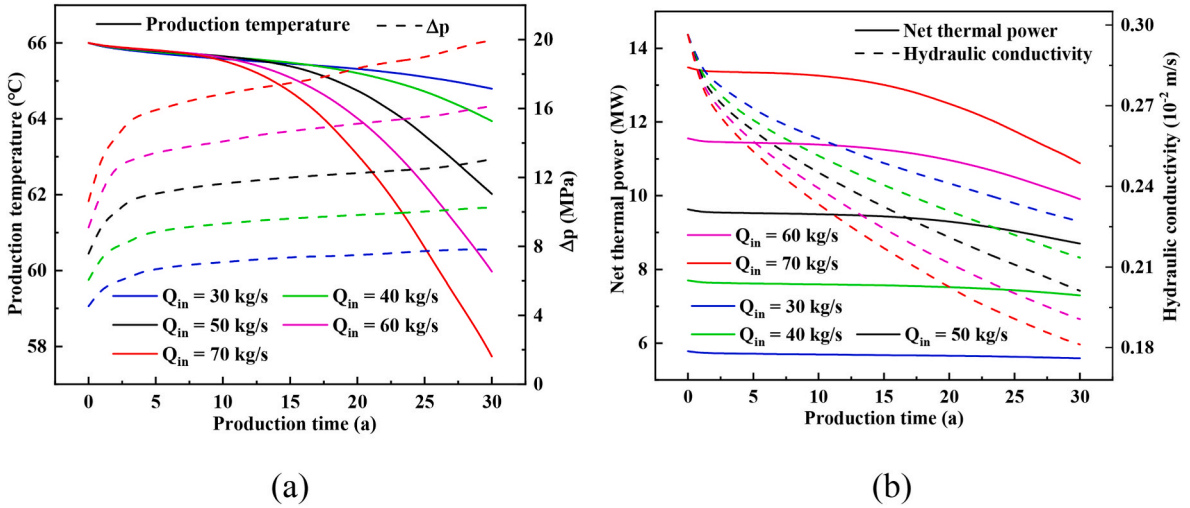

Fig. 9. The variation of (a) production temperature and pressure difference, and (b) net thermal power and Hydraulic conductivity with time at different Q_{in}.

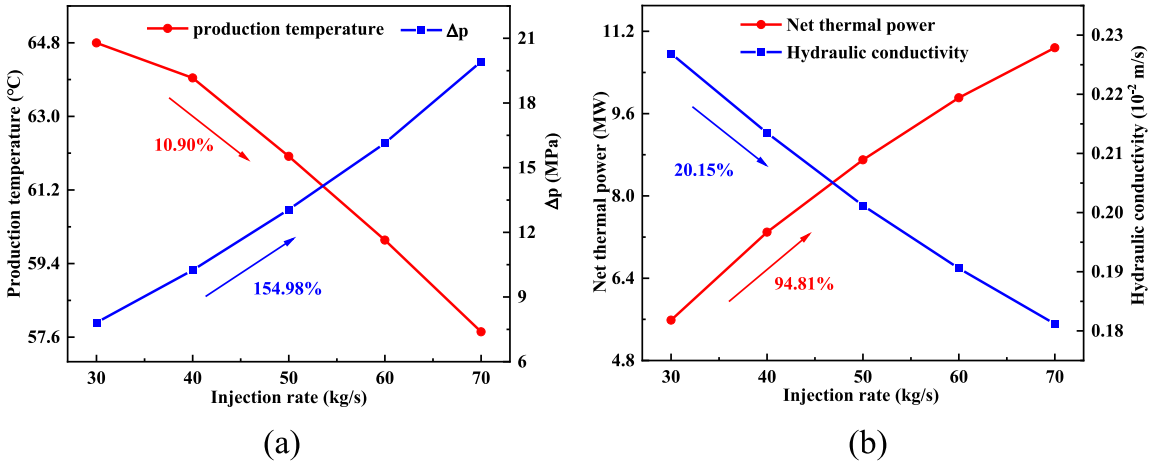

Fig. 10. The variation of (a) production temperature and pressure difference, and (b) net thermal power and Hydraulic conductivity with different Q_{in} after 30 years.

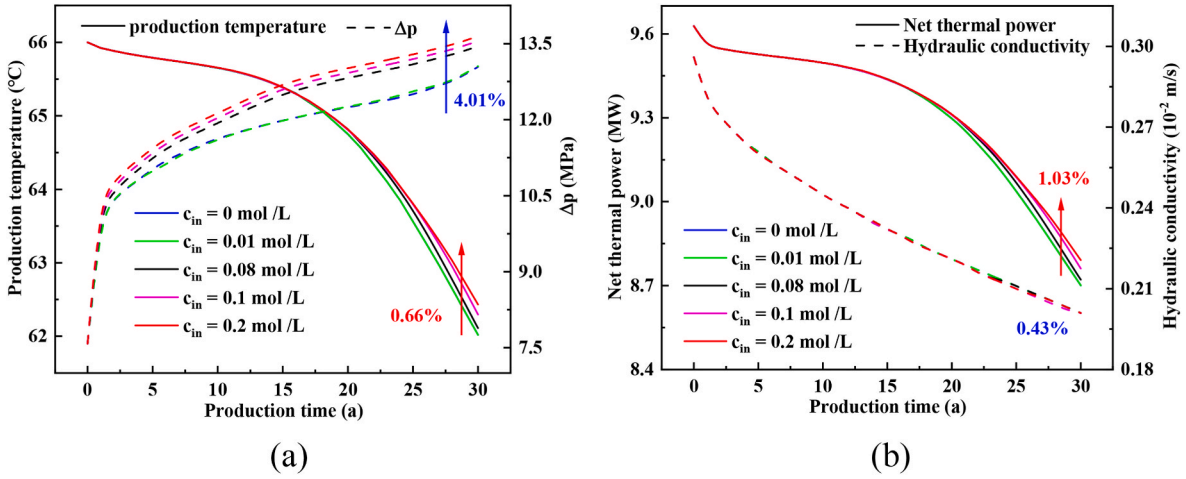

Fig. 11. The variation of (a) production temperature and pressure difference, and (b) net thermal power and Hydraulic conductivity with time at different c_{in}.

thermal power, the net thermal power is increased by 1.03% when the injection concentration increases from 0 mol/L to 0.2 mol/L. This is due to the little effect of the injection concentration on the production temperature. The hydraulic conductivity reduces with time and decreases with the injection concentration. However, the hydraulic conductivity is just decreased by 0.43% when the injection concentration increases from 0 mol/L to 0.2 mol/L. This is because the injection concentration only affects the area near the injection well and has little effect on the overall hydraulic conductivity of the reservoir.

From the above analysis, it is clear that the injection concentration has little effect on production temperature and hydraulic conductivity. Therefore, this section focuses on quantitatively analyzing the effect of injection concentration on pressure difference and net thermal power. The variation of pressure difference and net thermal power with c_{in} after 30 years is illustrated in Fig. 12. The equilibrium concentration of the solution is 0.084 mol/L under the initial reservoir conditions. The pressure difference is increased by 3.01% when the injection concentration rises from 0.01 mol/L to the equilibrium concentration, and the pressure difference is increased by 1.46% when the injection concentration rises from 0.084 mol/L to 0.2 mol/L. This suggests that the greater the difference between solution concentration and equilibrium concentration, the smaller the pressure difference under the condition of under-saturation injection and the greater the pressure difference under the condition of super-saturation injection. This is due to water-rock reactions near the injection well, the dissolution reactions are induced

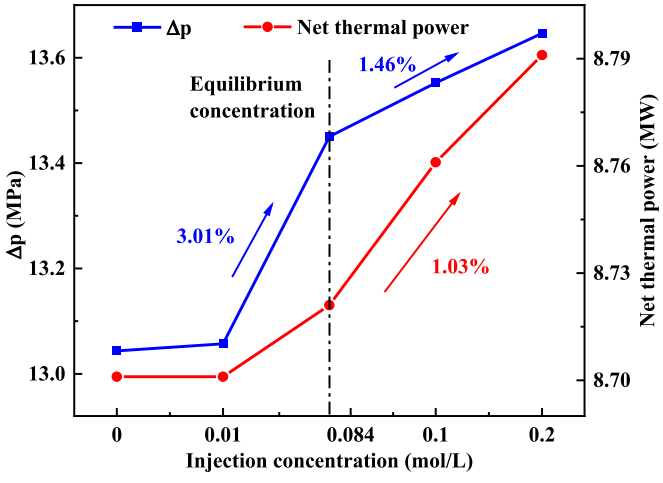

Fig. 12. The variation of pressure difference and net thermal power with c_{in} after 30 years.

under the undersaturated injection resulting in the pressure difference decrease, and the precipitation reaction occurs under the supersaturated injection resulting in the pressure difference increase. The net thermal power is increased by 1.03% when the injection concentration increases

from 0 mol/L to 0.2 mol/L. This is due to the production temperature increase with injection concentration. Compared to other parameters, it can be seen that the injection concentration has little impact on each parameter (production temperature, pressure difference, net thermal power, and hydraulic conductivity). This is because the water-rock reaction in the pore reduces its effect on the fracture deformation, thus reducing the effect on the heat thermal performance of the system.

4.2.4. The effect of "A_p/A_f"

According to Eqs. (9)–(19), the reaction and deformation rate is sensitive to the reaction-specific surface area. Meanwhile, the different specific surface areas of pores and fractures are the key factors for their different reaction mechanisms. The change in the thermal performance index over time at different A_p/A_f is illustrated in Fig. 13. The "A_p/A_f" has little effect on the production temperature and net thermal power, the production temperature and net thermal power are just increased by 0.15% and 0.24% when the "A_p/A_f" increases from 0.05 to 20. Due to the specific surface area of pores being adjusted to change the specific surface area ratio of pores and fractures in this paper, the variation of the "A_p/A_f" mainly affects the water-rock reaction in the pores. The water-rock reaction in the pore affects the fracture deformation and thus affects the thermal performance. However, the fluid has sufficient flow and heat transfer in the reservoir so that the production temperature and net thermal power vary little with the "A_p/A_f" in this case. The pressure difference increases with the "A_p/A_f" and is increased by 15.46% when the "A_p/A_f" increases from 0.05 to 20. This is due to the water-rock reaction rate in the pores increasing with the "A_p/A_f", but the water-rock reaction in the pore would induce the precipitation reaction in the fracture thus increasing the pressure difference. The relation of hydraulic conductivity with the "A_p/A_f" also proves this view. The hydraulic conductivity reduces with the "A_p/A_f" and is decreased by 8.86% when the"A_p/A_f" increases from 0.05 to 20. This further proves that the water-rock reaction in the pore will limit the water-rock reaction in the fracture, thus weakening the influence of the water-rock reaction on the thermal performance of the system.

From the above analysis, it is clear that the "A_p/A_f" has little effect on production temperature and net thermal power. This section mainly focuses on quantitatively analyzing the effect of the "A_p/A_f" on the pressure difference and hydraulic conductivity. Fig. 14 shows the variation of pressure difference and hydraulic conductivity in the 30th year with different "A_p/A_f". The change rate of the pressure difference is slow when the "A_p/A_f" is near "1", only 3.52%. The pressure difference is increased by 6.36% and 6.11% when the "A_p/A_f" increases from 0.05 to 0.5 and 2 to 20. The hydraulic conductivity is decreased by 9.79% when

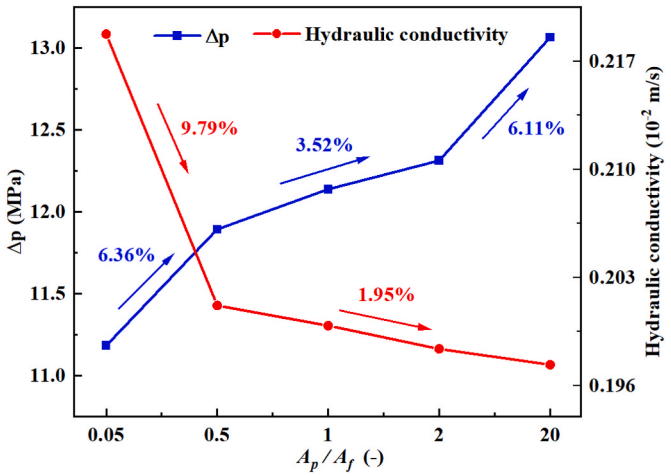

Fig. 14. The variation of pressure difference and net thermal power with "A_p/A_f" after 30 years.

the "A_p/A_f" increases from 0.05 to 0.5 and is decreased by 1.95% when the "A_p/A_f" increases from 0.5 to 20. This means that the water-rock reaction in the pore has an important effect on the water-rock reaction and deformation in the fracture. The water-rock reaction in the pores becomes weaker when the "A_p/A_f" is 0.5, which enhances the water-rock reaction in the fracture thus reducing the pressure difference and raising the hydraulic conductivity. The water-rock reaction in the fracture weakens speedily with the "A_p/A_f", even converse from a dissolution reaction to a precipitation reaction, thus rapidly increasing the pressure difference and reducing the hydraulic conductivity. From the above analysis, it can be seen that the "A_p/A_f" has a greater impact on the pressure difference and hydraulic conductivity and little impact on the production temperature and net thermal power. The "A_p/A_f" affects the fracture deformation mainly by affecting the reaction rate in the pore, and thus affects the thermal performance of the system.

4.3. Sensitivity analysis and evaluation

From the above analysis, there is a great influence of the injection temperature, injection displacement, and "A_p/A_f" on the thermal performance of the system. To further quantify the influence degrees of injection and reservoir parameters on thermal performance to specify the most important variables. Standard linear regression is employed to calculate the thermal performance of the system by increasing the value

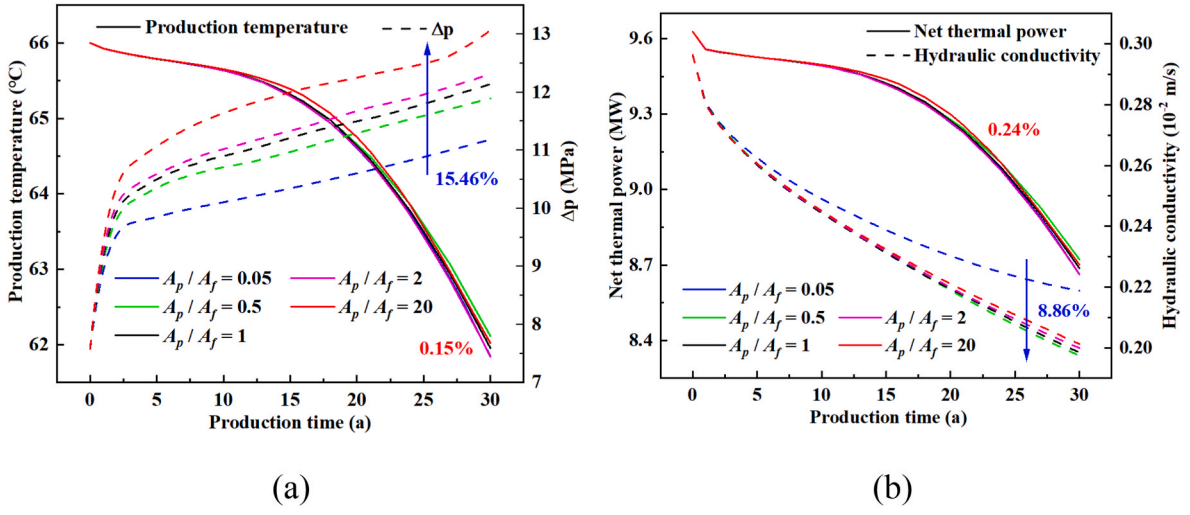

Fig. 13. The variation of (a) production temperature and pressure difference, and (b) net thermal power and Hydraulic conductivity with time at different "A_p/A_f".

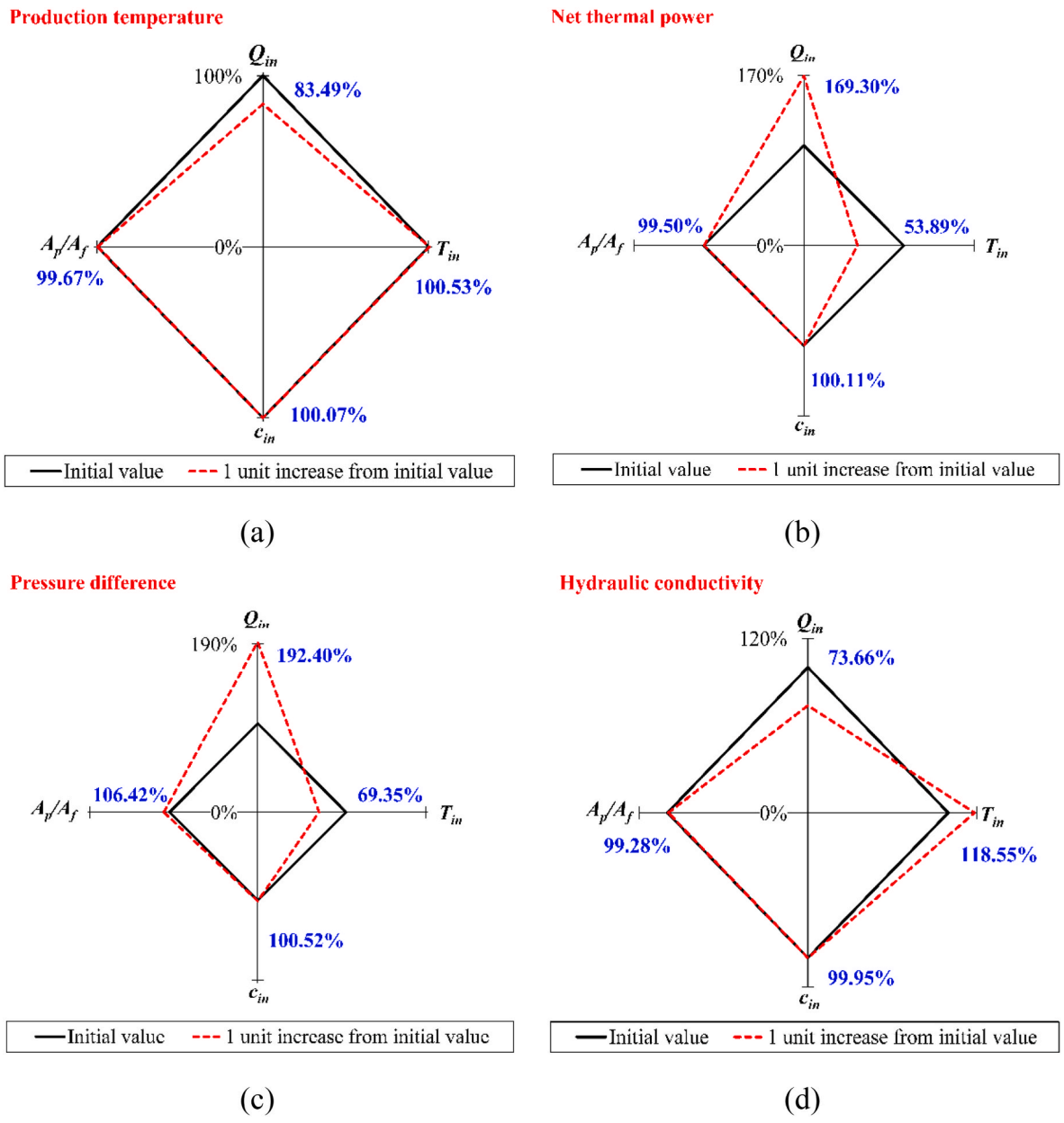

Fig. 15. Comparison of the influence of injection and reservoir parameters on the production temperature (a), net thermal power (b), pressure difference (c), and hydraulic conductivity (d).

of each key parameter by 1 unit [19]. Fig. 15 shows the comparison of the influence of injection and reservoir parameters on the (a) production temperature, (b) net thermal power, (c) pressure difference, and (d) hydraulic conductivity. It can be seen that the greatest impact on the production temperature is caused by Q_{in}, resulting in a 16.51% (1–83.49%) decrease in temperature when the Q_{in} increases by 1 unit. All key parameters, except for c_{in}, significantly impact the thermal performance, as shown in Fig. 15.

To quantify the relative contribution of each key parameter to the variation of thermal performance and identify the parameter with the most significant contribution. The relative contribution index is introduced, which is a single relative variation ratio (calculated from Fig. 15) divided by the sum of the relative variation ratio. As shown in Fig. 16 (a), the Q_{in} contributes 64% to the variation of production temperature among all four key parameters. The value is obtained by dividing 16.51% by (16.51% + 5.30% + 0.70% + 3.30%)×100%. Comparing the relative contribution index of each key parameter on thermal performance, it can be seen that the effect of Q_{in} on the production temperature is greater than T_{in} greater than "A_p/A_f" and greater than c_{in}. The net thermal power, pressure difference, and hydraulic conductivity are the same as the production temperature.

From the above analysis, it can be seen that the Q_{in} should be the primary consideration during the design and exploitation of the karst thermal reservoir, followed by the T_{in}, the "A_p/A_f ", and the c_{in}. Comparing the previous studies [19], the contribution rank of Q_{in} is the same as the previous study. On the contrary, the contribution index of the c_{in} obtained in this paper is significantly smaller than the previous results. This is due to the water-rock reaction in the pore causing the solution to change rapidly from the injected concentration to the equilibrium concentration, thus changing the water-rock reaction mechanism at the fracture surface(Concentration difference, temperature difference double drive to temperature difference drive). The water-rock reaction at the fracture surface is attenuated, thus mitigating the effect of injected concentration on thermal performance.

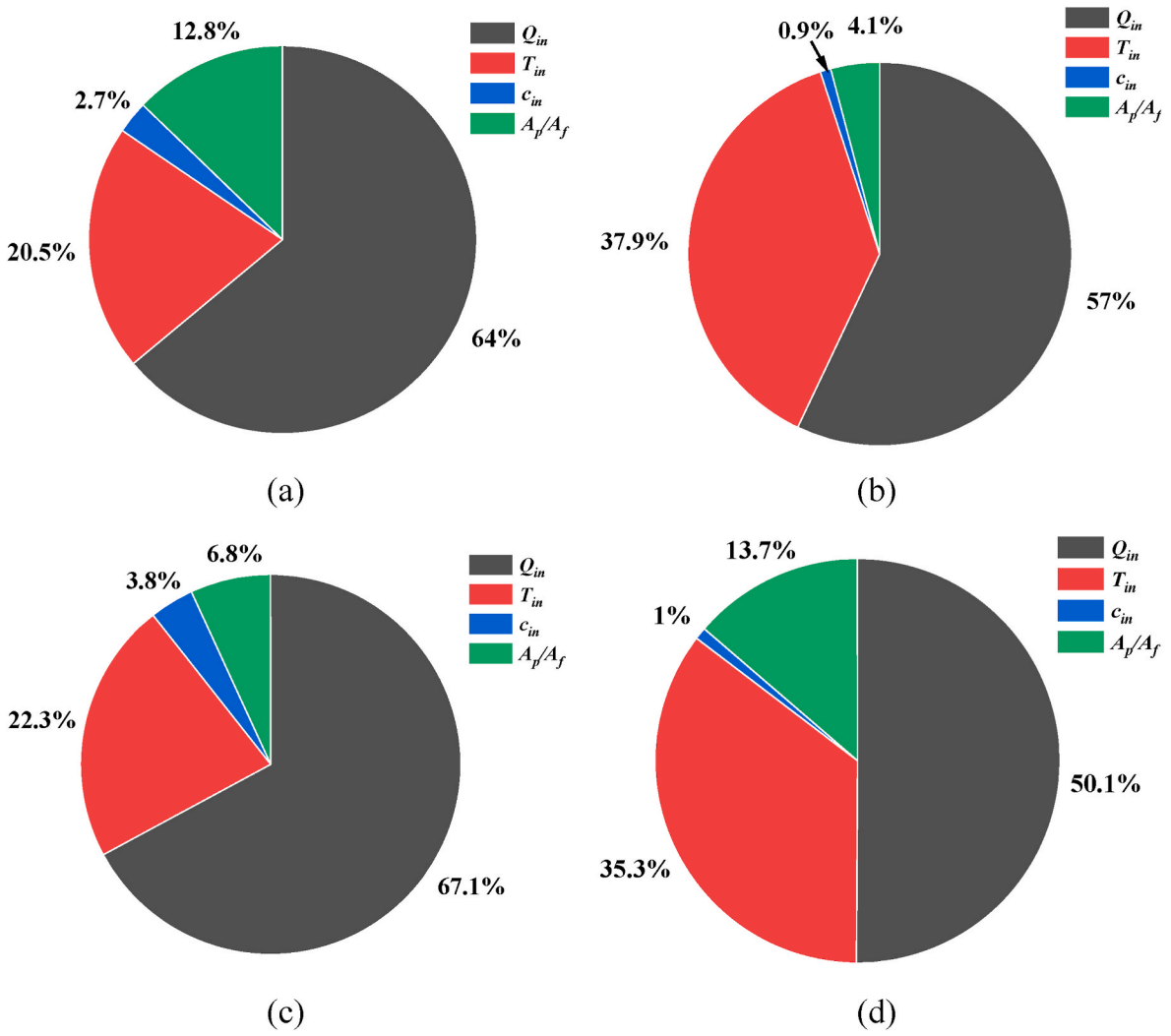

Fig. 16. The relative contribution percentage of injection and reservoir parameters to the change in (a) production temperature, (b) net thermal power, (c) pressure difference, and (d) hydraulic conductivity.

5. Conclusions

In this paper, a thermal-hydraulic-chemical coupling model considering dual media of pores and fracture is developed for the production of karst-based geothermal reservoirs under water-rock action. The importance of water-rock reactions in the pore is demonstrated, and the effect of the ratio of the reaction-specific surface area between pore and fracture (A_p/A_f) is investigated for the first time. Sensitivity evaluation is performed to quantitatively characterize the effect of each key parameter on the heat extraction performance of the karst-based geothermal reservoirs. The key findings provide a significant guide for accurate production prediction and exploitation of karst-based geothermal reservoirs, which are as follows:

The pore water-rock reaction affects the solution concentration, thus changing the fracture reaction mechanism, which results in a drastic effect on the reservoir hydraulic conductivity and pressure difference, even leading to an opposite trend.

The influence of water-rock reaction in pores on fracture deformation is regulated by A_p/A_f, which augments with A_p/A_f. The pressure difference increases and hydraulic conductivity decreases with A_p/A_f.

The effect of Q_{in} on the production temperature is greater than the T_{in} greater than A_p/A_f greater than the c_{in}. The net thermal power, pressure difference, and hydraulic conductivity are the same as the production temperature.

The Q_{in} should be the primary consideration during the design and exploitation of the system, followed by T_{in}, A_p/A_f, and c_{in}. The relative contribution of Q_{in} to T_{out}, N, Δp, and hydraulic conductivity are 64%, 57%, 67.1%, and 50.1%, respectively.

This study demonstrates the importance of water-rock reactions in the pore and investigates the effect of reservoir and engineering parameters on reservoir pores and fracture deformation and thermal performance. Future research should take into account the heteronomous properties and random fractures of karst-based geothermal reservoirs to build a model that is more conform to the real conditions of the reservoir.

CRediT authorship contribution statement

Jiayan Ji: Formal analysis, Methodology, Validation, Writing – original draft. **Xianzhi Song:** Conceptualization, Resources, Writing – original draft. **Junlin Yi:** Data curation, Writing – original draft, Writing – review & editing. **Guofeng Song:** Data curation, Writing – original draft, Writing – review & editing. **Gaosheng Wang:** Investigation, Methodology, Writing – review & editing.

Declaration of competing interest

The authors declare that they have no known competing financial

interests or personal relationships that could have appeared to influence the work reported in this paper.

Data availability

The authors do not have permission to share data.

Nomenclature

THMC	Thermal-hydraulic-mechanical-chemical
t	Time, s
u	Fluid velocity, m/s
k	Reservoir permeability, m^2
p	Pressure, Pa
d_f	Fracture aperture, m
g	Gravitational acceleration, m/s^2
T	Temperature, °C
$c_{p,f}$	Working fluid heat capacity, J/(kg·°C)
$c_{p,s}$	Heat capacity of the solid part in the reservoir, J/(kg·°C)
D_i	Effective diffusion coefficient of substance "i", m^2/s
c_i	Concentration of substance "i", mol/m^3
A_p	Specific surface areas of reservoir pores, 1/m
A_f	Specific surface areas of fracture, 1/m
f_c	Material transfer between matrix and fracture, dimensionless
R_i	Reaction rate of substance "i", $mol/(m^2 \cdot s)$
R	Molar gas constant, J/(mol·K)
Ea	Reaction activation energy, kj/mol
k^+	Reaction rate constants of carbonate, $mol/(m^2 \cdot s)$
SI	Saturation index, dimensionless
a_i	Activity of substance "i", mol/m^3
K_{eq}	Equilibrium constant, dimensionless
d_h	Hydraulic apertures, mm
d_{h0}	Initial hydraulic apertures, mm
d_{f0}	Initial fracture aperture, mm
f_f	Transformation coefficient, dimensionless
T_{out}	Production temperature, °C
T_{in}	Injection temperature, °C
p_{in}	Injection pressure, MPa
p_{out}	Production pressure, MPa
Q_{in}	Injection rate, kg/s
Q_{out}	Prodcution rate, kg/s
N	Net thermal power, MW
K	Hydraulic conductivity, m/s

Greek symbols

φ	Porosity, dimensionless
μ_f	Fluid dynamic viscosity, Pa·s
ρ_f	Fluid density, kg/m^3
λ_s	Heat conductivity of the solid part in the reservoir, W/(m·°C)
ρ_s	Density of solid component of the reservoir, kg/m^3
λ_f	Fluid heat conductivity, W/(m·K)
Δp	Injection-production pressure difference, MPa

Acknowledgments

The authors would like to acknowledge the National Natural Science Fund for Major Program of China (Grant No. 52192624), the National Science Fund for Distinguished Young Scholars of China, China (Grant No. 52125401).

References

[1] Wang G-l, Zhang W, Ma F, Lin W-j, Liang J-y, Zhu X. Overview on hydrothermal and hot dry rock researches in China. China Geology 2018;1(2):273–85.
[2] Zhu J, Hu K, Lu X, Huang X, Liu K, Wu X. A review of geothermal energy resources, development, and applications in China: Current status and prospects. Energy 2015;93:466–83.
[3] Hou J, Cao M, Liu P. Development and utilization of geothermal energy in China: current practices and future strategies. Renew Energy 2018;125:401–12.
[4] Hu Y, Cheng H, Tao S. Opportunity and challenges in large-scale geothermal energy exploitation in China. Crit Rev Environ Sci Technol 2022;52(21):3813–34.
[5] He Z, Feng J, Luo J, Zeng Y. Distribution, exploitation, and utilization of intermediate-to-deep geothermal resources in eastern China. Energy Geoscience 2023:100187.
[6] Zhu X, Wang G, Wang X, Qi S, Ma F, Zhang W, et al. Hydrogeochemical and isotopic analyses of deep geothermal fluids in the Wumishan formation in Xiong'an new area, China. Lithosphere 2022;2021(Special 5):2576752.
[7] Zhu Y, Li D, Hu Y, Zhang X, Li F, Ma F, et al. Deep structure of the Rongcheng geothermal field, Xiongan New Area: constraints from resistivity data and boreholes. Geothermics 2023;114:102776.
[8] Cui Y, Zhu C, Qiu N, Tang B, Guo S, Lu Z. The heat source origin of geothermal resources in Xiong'an new area, North China, in view of the influence of igneous rocks. Front Earth Sci 2022;10:818129.

[9] Li G, Ji J, Song X, Shi Y, Li S, Song Z, et al. Research advances in multi-field coupling model for geothermal reservoir heat extraction. Energy Rev 2022:100009.
[10] Lyu C, Liu J, Ren Y, Liang C, Zeng Y. Mechanical characteristics and permeability evolution of salt rock under thermal-hydro-mechanical (THM) coupling condition. Eng Geol 2022;302:106633.
[11] Shi Y, Xu F, Song X, Wang G, Zuo Y, Li X, et al. Rock damage evolution in the production process of the enhanced geothermal systems considering thermal-hydrological-mechanical and damage (THM-D). Energy 2023:129421.
[12] Song G, Song X, Xu F, Li G, Shi Y, Ji J. Contributions of thermo-poroelastic and chemical effects to the production of enhanced geothermal system based on thermo-hydro-mechanical-chemical modeling. J Clean Prod 2022;377:134471.
[13] Aliyu MD, Finkbeiner T, Chen H-P, Archer RA. A three-dimensional investigation of the thermoelastic effect in an enhanced geothermal system reservoir. Energy 2023;262:125466.
[14] Ontoy Y, Molling P, Xu T, Spycher N, Parini M, Pruess K. Scaling of hot brine injection wells: supplementing field studies with reactive transport modeling. Conference Scaling of hot brine injection wells: supplementing field studies with reactive transport modeling. p. 12-14..
[15] Xu T, Ontoy Y, Molling P, Spycher N, Parini M, Pruess K. Reactive transport modeling of injection well scaling and acidizing at Tiwi field, Philippines. Geothermics 2004;33(4):477–91.
[16] Rawal C, Ghassemi A. A reactive thermo-poroelastic analysis of water injection into an enhanced geothermal reservoir. Geothermics 2014;50:10–23.
[17] André L, Rabemanana V, Vuataz F-D. Influence of water–rock interactions on fracture permeability of the deep reservoir at Soultz-sous-Forêts. France. Geothermics. 2006;35(5–6):507–31.
[18] Pandey S, Chaudhuri A, Rajaram H, Kelkar S. Fracture transmissivity evolution due to silica dissolution/precipitation during geothermal heat extraction. Geothermics 2015;57:111–26.
[19] Song G, Song X, Xu F, Li G, Wang G, Ji J, et al. Numerical parametric investigation of thermal extraction from the enhanced geothermal system based on the thermal-hydraulic-chemical coupling model. J Clean Prod 2022;352:131609.
[20] Song G, Song X, Ji J, Wu X, Li G, Xu F, et al. Evolution of fracture aperture and thermal productivity influenced by chemical reaction in enhanced geothermal system. Renew Energy 2022;186:126–42.
[21] Chen Y, Ma G, Wang H. The simulation of thermo-hydro-chemical coupled heat extraction process in fractured geothermal reservoir. Appl Therm Eng 2018;143:859–70.
[22] Ji J, Song X, Song G, Xu F, Shi Y, Lv Z, et al. Study on fracture evolution model of the enhanced geothermal system under thermal-hydraulic-chemical-deformation coupling. Energy 2023;269:126604.
[23] Ji J, Song X, Li S, Xu F, Song G, Shi Y, et al. Study on the effect of fracture morphology on fracture deformation based on the thermal-hydraulic-chemical-deformation coupling model. Energy 2023;282:128628.
[24] Jing Z, Watanabe K, Willis-Richards J, Hashida T. A 3-D water/rock chemical interaction model for prediction of HDR/HWR geothermal reservoir performance. Geothermics 2002;31(1):1–28.
[25] Pandey SN, Chaudhuri A. The effect of heterogeneity on heat extraction and transmissivity evolution in a carbonate reservoir: a thermo-hydro-chemical study. Geothermics 2017;69:45–54.
[26] Cheng W-L, Wang C-L, Nian Y-L, Han B-B, Liu J. Analysis of influencing factors of heat extraction from enhanced geothermal systems considering water losses. Energy 2016;115:274–88.
[27] Pruess K. Enhanced geothermal systems (EGS) using CO2 as working fluid—a novel approach for generating renewable energy with simultaneous sequestration of carbon. Geothermics 2006;35(4):351–67.
[28] Xu T, Apps JA, Pruess K, Yamamoto H. Numerical modeling of injection and mineral trapping of CO2 with H2S and SO2 in a sandstone formation. Chem Geol 2007;242(3):319–46.
[29] Witherspoon P, Amick C, Gale J, Iwai K. Observations of a potential size effect in experimental determination of the hydraulic properties of fractures. Water Resour Res 1979;15(5):1142–6.
[30] Song X, Shi Y, Li G, Yang R, Wang G, Zheng R, et al. Numerical simulation of heat extraction performance in enhanced geothermal system with multilateral wells. Appl Energy 2018;218:325–37.
[31] Pandey SN, Chaudhuri A, Rajaram H, Kelkar S. Fracture transmissivity evolution due to silica dissolution/precipitation during geothermal heat extraction. Geothermics 2015;57:111–26.
[32] Pandey SN, Chaudhuri A, Kelkar S, Sandeep VR, Rajaram H. Investigation of permeability alteration of fractured limestone reservoir due to geothermal heat extraction using three-dimensional thermo-hydro-chemical (THC) model. Geothermics 2014;51:46–62.
[33] Yao J, Huang Z-Q. Fractured vuggy carbonate reservoir simulation. Springer; 2017.
[34] Jiayan J, Xianzhi S, Fuqiang X, Guofeng S, Yu S, Gaosheng W, et al. Effects of variable thermophysical properties of water on the heat extraction of an enhanced geothermal system: a numerical case study. Appl Therm Eng 2022;217:119050.
[35] Mahmoodpour S, Singh M, Turan A, Bär K, Sass I. Hydro-thermal modeling for geothermal energy extraction from Soultz-sous-Forêts. France. Geosciences 2021;11(11):464.
[36] Lai P, Moulton K, Krevor S. Pore-scale heterogeneity in the mineral distribution and reactive surface area of porous rocks. Chem Geol 2015;411:260–73.
[37] Zhonghe P, Yanlong K, Jumei P, Shengbiao H, Jiyang W. Geothermal resources and development in Xiongan new area. Bull Chin Acad Sci 2017;32(11):1224–30.
[38] Wang G-l, Wang W-l, Zhang W, Ma F, Liu F. The status quo and prospect of geothermal resources exploration and development in Beijing-Tianj in-Hebei region in China. China Geology 2020;3(1):173–81.
[39] Lv C, Tang C-S, Zhu C, Li W-Q, Chen T-Y, Zhao L, et al. Environmental dependence of microbially induced calcium carbonate crystal precipitations: experimental evidence and insights. J Geotech Geoenviron Eng 2022;148(7):04022050.
[40] Blanc P, Lassin A, Piantone P, Azaroual M, Jacquemet N, Fabbri A, et al. Thermoddem: a geochemical database focused on low temperature water/rock interactions and waste materials. Appl Geochem 2012;27(10):2107–16.
[41] Wilson JL, Miller PJ. Two-dimensional plume in uniform ground-water flow. J Hydraul Div 1978;104(4):503–14.